Paleoceanography and Paleoclimatology

RESEARCH ARTICLE
10.1029/2020PA004091

Key Points:

- Diatom *sed*aDNA composition is concordant with reconstructed sea-ice dynamics, SSTs, and subsurface salinities over the last millennia
- Loss of diatom richness at ~11.1 cal kyr BP is possibly a consequence of increased freshwater input from Kamchatka
- Shifts of potential ecotypes of species from the genus *Chaetoceros* with changing environmental conditions

Supporting Information:

Supporting Information may be found in the online version of this article.

Correspondence to:

H. H. Zimmermann and U. Herzschuh, heike.zimmermann@awi.de; ulrike.herzschuh@awi.de

Citation:

Zimmermann, H. H., Stoof-Leichsenring, K. R., Kruse, S., Nürnberg, D., Tiedemann, R., & Herzschuh, U. (2021). Sedimentary ancient DNA from the subarctic North Pacific: How sea ice, salinity, and insolation dynamics have shaped diatom composition and richness over the past 20,000 years. *Paleoceanography and Paleoclimatology*, *36*, e2020PA004091. https://doi.org/10.1029/2020PA004091

Received 18 AUG 2020
Accepted 21 MAR 2021

Sedimentary Ancient DNA From the Subarctic North Pacific: How Sea Ice, Salinity, and Insolation Dynamics Have Shaped Diatom Composition and Richness Over the Past 20,000 Years

H. H. Zimmermann[1], K. R. Stoof-Leichsenring[1], S. Kruse[1], D. Nürnberg[2], R. Tiedemann[3], and U. Herzschuh[1,4,5]

[1]Polar Terrestrial Environmental Systems, Alfred Wegener Institute Helmholtz Centre for Polar and Marine Research, Potsdam, Germany, [2]Ocean Circulation and Climate Dynamics, GEOMAR Helmholtz Centre for Ocean Research Kiel, Kiel, Germany, [3]Marine Geology, Alfred Wegener Institute Helmholtz Centre for Polar and Marine Research, Bremerhaven, Germany, [4]Institute of Biochemistry and Biology, University of Potsdam, Potsdam, Germany, [5]Institute of Environmental Sciences and Geography, University of Potsdam, Potsdam, Germany

Abstract We traced diatom composition and diversity through time using diatom-derived sedimentary ancient DNA (*sed*aDNA) from eastern continental slope sediments off Kamchatka (North Pacific) by applying a short, diatom-specific marker on 63 samples in a DNA metabarcoding approach. The sequences were assigned to diatoms that are common in the area and characteristic of cold water. *Sed*aDNA allowed us to observe shifts of potential lineages from species of the genus *Chaetoceros* that can be related to different climatic phases, suggesting that pre-adapted ecotypes might have played a role in the long-term success of species in areas of changing environmental conditions. These *sed*aDNA results complement our understanding of the long-term history of diatom assemblages and their general relationship to environmental conditions of the past. Sea-ice diatoms (*Pauliella taeniata* [Grunow] Round & Basson, *Attheya septentrionalis* [Østrup] R. M. Crawford and *Nitzschia frigida* [Grunow]) detected during the late glacial and Younger Dryas are in agreement with previous sea-ice reconstructions. A positive correlation between pennate diatom richness and the sea-ice proxy IP_{25} suggests that sea ice fosters pennate diatom richness, whereas a negative correlation with June insolation and temperature points to unfavorable conditions during the Holocene. A sharp increase in proportions of freshwater diatoms at ~11.1 cal kyr BP implies the influence of terrestrial runoff and coincides with the loss of 42% of diatom sequence variants. We assume that reduced salinity at this time stabilized vertical stratification which limited the replenishment of nutrients in the euphotic zone.

1. Introduction

Climate warming is transforming arctic and subarctic ecosystems by a reduction in the duration, extent, and thickness of sea ice (Parkinson et al., 1999; Walsh et al., 2017)—a key variable of the global climate system whose disappearance is resulting in a positive temperature feedback from a reduction of the surface albedo (Pistone et al., 2014). Rapidly melting glaciers and increased riverine runoff resulting from thawing permafrost and augmented precipitation over the adjacent continents are expected to decrease sea-surface salinities, for example, by about 1.5 ± 1.1 psu on average in the Arctic Ocean (Shu et al., 2018). As a consequence, the fresher, less dense water masses are expected to enhance vertical water-column stratification, which could result in a reduced supply of nutrients to the euphotic zone (Tremblay & Gagnon, 2009). On top of the regionally expected loss of sea ice-associated organisms, such a scenario could potentially affect the distribution, composition, and diversity of primary producers which are limited by the availability of nutrients, amongst others, with unknown consequences for food-web structure, biochemical cycles, and the biological carbon pump (Coupel et al., 2015; Li et al., 2009).

The subarctic northwest (NW) Pacific and its adjacent seas have experienced pronounced environmental changes since the Last Glacial Maximum (LGM). The variability of previously reconstructed sea-surface temperatures and sea-ice coverage has been connected to the millennial-scale climatic changes recorded in sediment cores from the North Atlantic and in Greenland ice cores (Max et al., 2012a; Méheust et al., 2016).

Several meltwater pulses have been detected in sediment cores of this region (Gorbarenko et al., 2019), which make it attractive for analyzing the effects of past environmental changes on primary producers.

A dominant group of primary producers in high-latitudinal sea-ice and coastal ecosystems are diatoms (Poulin et al., 2011), which are single-celled eukaryotes that form a cell wall of biomineralized silicon dioxide (biogenic silica) and fix carbon dioxide as a product of their photosynthetic activity (Rotatore et al., 1995). They are sensitive to environmental change and can be used as indicators of past sea-surface conditions. For example, compositional data of diatom microfossil assemblages of the subarctic NW Pacific and the Bering and Okhotsk Seas have revealed variations in ocean circulation patterns, past distribution of sea ice, and past sea-surface temperatures (Caissie et al., 2010; Ren et al., 2009; Sancetta, 1979; Sancetta & Silvestri, 1986; Smirnova et al., 2015). Yet, some questions cannot be addressed with assemblage data, for example, whether intra-specific variants could be linked to different environmental conditions.

The past decade has brought forward genetic surveys which have revealed substantially concealed diversity in diatoms, showing that widely distributed species can have ecotypes associated with, for example, different growth optima (Hamsher et al., 2013) that may not be detected morphologically (cryptic diversity) or only by exhaustive analysis (pseudo-cryptic) (Degerlund et al., 2012). In this regard, the analysis of *sed*aDNA is an advantage. Recently, *sed*aDNA was used as a proxy for sea-ice reconstructions by targeting diatom *sed*aDNA composition in Fram Strait (Zimmermann et al., 2019), for tracing a sea-ice dinoflagellate east of Greenland (De Schepper et al., 2019) and to identify changes of ocean circulation patterns by targeting diatoms and non-fossilized foraminifers east of Svalbard (Pawłowska, Łącka, et al., 2020). Ancient DNA has profound advantages. First, it can detect species that are absent from microfossil records either due to dissolution or because they lack a biomineralized cell wall. Second, it allows for the detection of (pseudo-) cryptic diversity in morphological species complexes, which might be adapted to different ecological conditions. However, ancient DNA is usually highly fragmented and degraded post-mortem (Pääbo, 1989) during its way to the seafloor depending amongst others on water depth, organic matter load, temperature, salinity and redox potential (Corinaldesi et al., 2008) and post-burial due to enzymatic and microbial activity (Corinaldesi et al., 2008; Dell'Anno et al., 2002). Hence, for DNA metabarcoding of diatoms, the marker should ideally target a short sequence stretch, and additionally avoid co-amplification of other taxonomic groups or co-amplification of highly similar paralogs. Targeting a part of the gene encoding for the large subunit of the RuBisCO (*rbcL*) on the chloroplast genome of diatoms is of advantage. The variability of the *rbcL* gene allows detection of diatoms to species level (Rimet et al., 2019), and is amongst the most applied barcoding genes; thus, it has a substantial reference database (Rimet et al., 2019; Zimmermann et al., 2014).

Our aim is to trace temporal changes of diatom *sed*aDNA composition and diversity over the past 19.9 cal kyr BP, and to relate changes to environmental conditions to answer the following questions: (1) How has diatom composition changed since the LGM? And how are such changes related to past sea-ice conditions, subsurface salinities, and incoming solar radiation (insolation)? (2) How did diatom *sed*aDNA richness change over time?

2. Materials and Methods

2.1. Study Site

The sediment core SO201-2-12KL (N 53.993, E 162.376, depth = 2,173 m) was collected from the Kamchatka Strait near Kronotskii Peninsula at the eastern continental slope of Kamchatka, where the shelf area is very narrow (Figure 1). The study area is influenced by water masses transported via the East Kamchatka Current, which brings nutrient-rich waters from the Bering Sea to the subarctic North Pacific Ocean (Stabeno et al., 1999) and by the Alaskan Stream, which transports water masses from the Gulf of Alaska along the Aleutian Arc and water from the wind-driven, cyclonic western subarctic gyre (Nagano et al., 2016; Stabeno & Reed, 1994). As evaporation is lower than precipitation and runoff from Kamchatka, the water column is characterized by a stable halocline (Gebhardt et al., 2008). Modern sea-surface temperatures in the area are about 1°C in winter and range between 6°C and 10°C in summer (Riethdorf et al., 2013a) with winter sea-ice formation only along the coast of Kamchatka (Matul' et al., 2015), but is influenced by drifting sea ice (Polyakova, 2007).

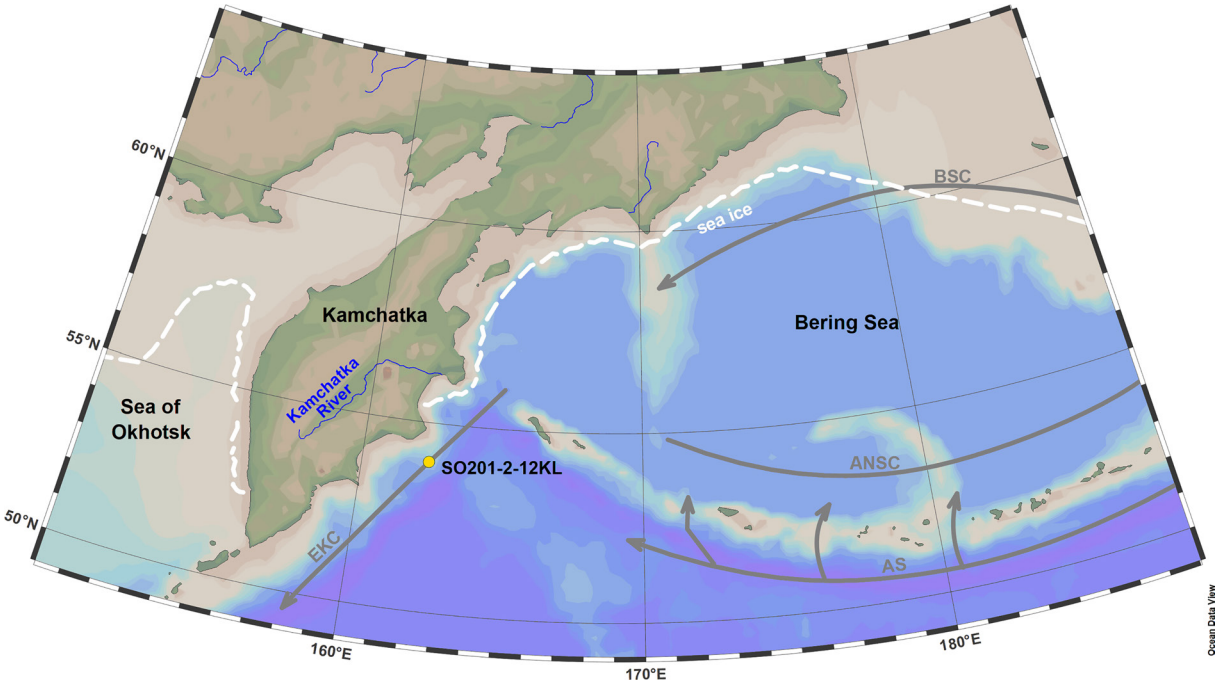

Figure 1. Map showing the study area with surface current patterns (EKC, East Kamchatka Current; AS, Alaskan Stream; ANSC, Aleutian North Slope Current; BSC, Bering Sea Current) indicated by gray arrows and the coring site SO201-2-12 KL marked by a yellow dot. The white dashed line represents the median sea-ice extent in March between 1981 and 2010 (Fetterer et al., 2017). The map was produced with Ocean Data View (Schlitzer, 2002).

2.2. Sample Material

Sediment material was retrieved with a piston corer (SO201-2-12KL) during RV Sonne cruise SO-201 (KALMAR) in 2009 (Max et al., 2012a). The sediment core is 9.05-m long and mostly composed of sandy-silty-clayey mud. We here rely on the chronostratigraphy established by (Max et al., 2012a), which is based on radiocarbon ages derived from *Neogloboquadrina pachyderma* sinistral and correlations of X-ray fluorescence data as well as color and light reflectance properties from sediment cores of the Western Bering Sea, the Okhotsk Sea, and the subarctic Northwest Pacific. Core material was stored at 4°C since retrieval. Samples for ancient DNA analyses were collected in 2018 at GEOMAR, Kiel, in a laboratory devoid of any molecular biology work. We collected a sample every ~16 cm (but as we included samples processed in a pilot project, there are some instances where an additional sample was included) with a median temporal resolution of 240 years (Levitan et al., 2015). To avoid the contamination of the samples with modern DNA, sampling was performed from the oldest to the youngest samples while wearing a plastic coverall, face mask, hair net. Gloves were changed between each sample. The treatment of the equipment and the sampling procedure for ancient DNA analyses followed the protocol for non-frozen sediment cores explained in Epp et al. (2019).

2.3. DNA Extraction and Concentration

The DNA extractions, PCR setups, and reaction conditions were carried out in a dedicated laboratory for ancient DNA at AWI Potsdam, while PCRs and downstream preparations for sequencing were carried out in the genetics laboratories located in another building. Total DNA was extracted using the DNeasy PowerMax Soil kit (Qiagen) as described in Zimmermann et al. (2017) from 63 samples (2–4 ml sediment). Each extraction batch contained up to nine samples and one negative control (in total seven negative controls). Subsequently, we measured the total DNA concentration on a Qubit 4.0 fluorometer (Invitrogen) using the Qubit dsDNA BR Assay Kit (Invitrogen). We concentrated for each sample 600 µl of the extracted DNA using the GeneJET PCR Purification KIT (Thermo Fisher Scientific) and eluted twice with 15-µl elution buffer to retain a final volume of ~30 µl. The DNA concentration was measured again and the DNA was diluted to 3 ng/µl. The DNA extracts and aliquots were stored at −20°C.

2.4. *Sed*aDNA Metabarcoding

*Sed*aDNA metabarcoding was carried out using the rbcl_76 marker, which was designed for both marine and freshwater species (Stoof-Leichsenring et al., 2012), and which is well suited for ancient and degraded samples due to its short target sequence (76 bp). Amplifications were carried out using the primers Diat_rbcL_705F (AACAGGTGAAGTTAAAGGTTCATAYTT) and Diat_rbcL_808R (TGTAACCCATAACTAAATCGATCAT), which were tagged for parallel sequencing (Binladen et al., 2007) as described in Dulias et al. (2017) and Huang et al. (2020). The PCR reaction mixes and conditions were prepared according to the adjusted protocol for tagged Diat_rbcL_705F and Diat_rbcL_808R primers as described in Dulias et al. (2017) with the exception that 3-µl DNA (DNA concentration 3 ng/µl) was used as a template. PCRs were carried out under the following conditions: 5 min at 94°C (initial denaturation), then 50 cycles at 94°C (denaturation), 49°C (annealing) and 68°C (elongation) and a final elongation step at 72°C for 5 min. Each PCR batch was composed of one extraction batch (nine samples and the corresponding extraction negative control) and a PCR negative control. Furthermore, each PCR batch was subjected to three independent PCRs, with distinct primer-tag combinations on different days. PCR success was checked with gel-electrophoresis. Subsequently, the PCR products including all negative controls were purified using the MinElute Purification Kit (Qiagen). The DNA concentrations of the PCR products were measured again with the Qubit dsDNA BR Assay Kit and mixed in equal concentrations. As negative controls were below detection limit, 10 µl for negative controls were added to the sample pool. The sample pool was sent to Fasteris SA sequencing service (Switzerland) who carried out library preparation with the Mid Output Kit v. 2 according to the Fasteris Metafast protocol and sequencing (2 × 150 bp, paired-end) on the Illumina NextSeq 500 platform (Illumina Inc.). The sequences are deposited at Dryad (Zimmermann, Stoof-Leichsenring, Kruse, Nuernberg, et al., 2020, Zimmermann, Stoof-Leichsenring, Kruse, Müller, et al., 2020).

2.5. Bioinformatic Processing

The sequence reads were processed, filtered, and assigned a taxonomic name according to the NCBI taxonomy using the OBITools package (Boyer et al., 2016) with the same bioinformatics parameter settings as described in Dulias et al. (2017). Taxonomic assignment of amplicon sequence variants (ASVs) (Callahan et al., 2017) was applied via the EMBL nucleotide reference database (EMBL release 138 from November 2018; Kanz et al., 2005) using a least common ancestor approach implemented in OBITools (Table S1). The resulting table was combined with samples sequenced on a previous run (Zimmermann, Stoof-Leichsenring, Kruse, Nuernberg, et al., 2020; Zimmermann, Stoof-Leichsenring, Kruse, Müller, et al., 2020). Ancient DNA is characterized by accumulation of post-mortem damage over time (Gilbert et al., 2003), which might be increased due to long-term storage at 4°C before *sed*aDNA sample collection. After amplification with PCR, sequences that contain damaged sites occur in the data as variants of the original sequence, thereby inflating richness estimates (Figure S2). To account for this, we used stringent filter criteria, thus, further denoising was carried out on the combined data set using R v. 3.6.0 (R Core Team, 2018): PCR and sequencing errors are known to inflate diversity estimates, especially with ancient DNA; hence, we kept only those ASVs that (1) were assigned a taxonomic name based on 90%–100% similarity to an entry in the reference database, (2) were represented with at least 100 read counts in total and (3) at least 10 read counts per PCR-product, (4) were present at least three times among all PCR-products, (5) showed taxonomic resolution at least to phylum level "Bacillariophyta", and (6) were tagged as "internal" by *obiclean* in less than 50% of the different replicates per sample. If two sequences differ from each other by one nucleotide, *obiclean* uses the count information of each variant and the more abundant one is tagged as "head" while the less abundant one(s) are tagged as "internal" (Boyer et al., 2016). After filtering, the PCR replicates of a sample were combined and subjected to rarefaction. We resampled the data based on the minimum number of sequences (8,882 counts) using a custom R script (https://github.com/StefanKruse/R_Rarefaction; Kruse, 2019).

The negative controls were mostly clean (Table S2). They contained, on average, 38 sequence variants of which 90.4% occurred with only one or two read counts, which can most likely be attributed to tag jumps (Schnell et al., 2015). Only one PCR-product of an extraction negative control contained more reads, which was probably a pipetting mistake during PCR-setup, because the corresponding PCR negative control was clean and the other two PCR replicates of this negative control were clean as well.

2.6. Statistical Analysis

2.6.1. Composition

Constrained hierarchical clustering (CONISS; Grimm, 1987) was applied in which clusters were constrained stratigraphically by sample depth with the *chclust*-function from the R package "rioja" v. 0.9-21 (Juggins, 2012). Subsequently, we used the bstick-function from the "vegan" package v. 2.5-6 (Oksanen et al., 2011) to compare the dispersion of the computed classification against the dispersion of a broken stick model in order to assess the number of significant zones. The stratigraphic diagram was plotted using *strat.plot* from "rioja" and based only on ASVs having proportions of at least 1% in the data set.

2.6.2. Environmental Variables

Environmental variables from the same core were retrieved from PANGAEA and included IP_{25} concentrations indicative of ice-edge conditions (Méheust et al., 2015), biogenic opal as proxy for primary productivity (Max et al., 2012b), foraminifer-derived reconstruction of local, ice-volume corrected seawater oxygen isotope composition ($\delta^{18}O_{ivc\text{-}sw}$) as proxy for salinity (Riethdorf et al., 2013b), and the branched and isoprenoid tetraether (BIT) index, measuring the relative input of terrestrial and marine glycerol dialkyl glycerol tetraethers (GDGTs; Meyer et al., 2016a). Furthermore, we used NGRIP 20 years means of $\delta^{18}O$ (http://www.iceandclimate.nbi.ku.dk/data/2010-11-19_GICC05modelext_for_NGRIP.txt) as independent Northern Hemisphere temperature proxy, and June insolation was calculated after Laskar et al. (2004). Environmental variables were interpolated using the methods described in Reschke et al. (2019). First, the variables were transformed using the function *zoo* from the "zoo" package v. 1.8-7 and used in the function *CorIrregTimser* using the package "corit" v. 0.0.0.9000 (https://github.com/EarthSystemDiagnostics/corit). As environmental data were limited, we focused the multivariate analyses (package "vegan") on the temporal interval from 7.56–16.48 cal kyr BP and applied a *z*-score transformation using function *scale*. ASVs with proportions of at least 1.5% were selected for multivariate statistical analysis. To avoid double-zeros being regarded as similar between samples, we used Hellinger transformation on the reduced proportion-based community matrix with *decostand* from "vegan".

To test for linear dependencies of the environmental variables, we ran a redundancy analysis (RDA) using function *rda* and used this as input to calculate the variance inflation factor (VIF) using the *vif.cca* function. Based on VIFs exceeding 10 and thus collinearity with other variables, we stepwise excluded biogenic opal, NGRIP $\delta^{18}O$, and the BIT-index from the set of variables. Then, we applied forward selection using *ordistep* for stepwise extension of the regression model and performed a permutation test using *RsquareAdj* to keep variables that significantly explain some of the variances of the community matrix. Subsequently, we tested the chosen variables with conditional variables for their unique explained variance as forward selection depends on the order by which the variables were put into the model.

2.6.3. Taxonomic Richness and Beta-Diversity

Richness, the number of ASVs, was calculated as a measure of taxonomic alpha-diversity using the *estimateD* function from the iNEXT package v. 2.0.20 (Hsieh et al., 2016), which allowed rarefaction analysis for both centric and pennate diatom ASVs in parallel. Rarefied richness was tested for correlations with interpolated environmental variables using *rcorr* from the package "Hmisc" v. 4.4-0 (Harrell Jr, 2020) with the method "Pearson". Taxonomic beta-diversity was calculated using the *betapart.core* and *beta.pair* functions of the "betapart" v. 1.5.1 package (Baselga & Orme, 2012), which allowed the split of pair-wise Jaccard dissimilarities into nestedness (sample composition is a subset of the previous sample composition) and turnover fractions (taxonomic replacement from one sample to the next). All analyses were carried out using R v. 3.6.0 (R Core Team, 2018).

3. Results

A total of 13,584,296 reads were assigned to 3,038 ASVs at 90%–100% similarity to reference sequences. Of these, 2,191 ASVs were specific for diatoms and comprised 11,746,154 reads. After further filtering, 11,114,776 reads remained assigned to 232 ASVs, which amounts to 94.6% of all reads assigned to diatoms. Of these, 47% are resolved to species level and 38% to genus level. The lowest number of diatom read counts (8,882 counts) was detected in the sample at 7.885-m depth (18.0 cal kyr BP), while the highest number

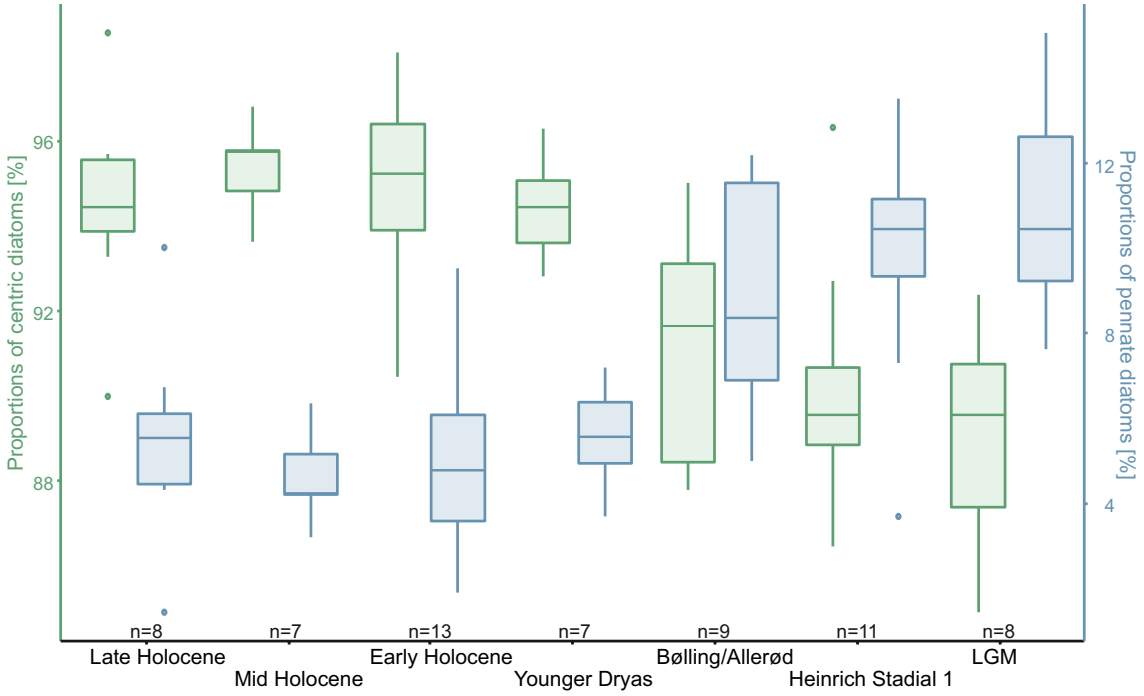

Figure 2. Proportions of amplicon sequence variants assigned to centric diatoms (green) and pennate diatoms (blue) during the glacial/interglacial transition over the past 19.9 cal kyr BP.

(914,117 counts) was detected in the sample at 3.0 m (11.1 cal kyr BP). The majority of diatom-derived reads were assigned to centric diatoms (92.7%), while 7.3% of reads were assigned to pennate diatoms. The sequence variants were assigned to 25 different families, of which Bacillariaceae (68 ASVs), Chaetocerotaceae (40 ASVs), Naviculaceae (18 ASVs), and Thalassiosiraceae (54 ASVs) encompassed the majority of the 231 ASVs that remained after filtering and rarefaction.

3.1. Diatom *sed*aDNA Composition

Throughout the past 19.9 cal kyr BP the sedaDNA composition of the 63 samples is dominated by ASVs assigned to cold-water and sea ice-associated species, such as *Bacterosira* sp., *Nitzschia* (cf.) *frigida*, *Porosira* sp., *Thalassiosira antarctica,* and *T. nordenskioeldii*. Dominant ASVs are assigned to centric diatoms of the genera *Chaetoceros*, *Thalassiosira*, *Porosira,* and *Skeletonema*.

The proportions of ASVs assigned to pennate diatoms per sample ranges between a minimum of 1.4% (2.36 cal kyr BP) and a maximum of 15.1% (19.9 cal kyr BP). Pennate diatoms, predominantly pennate, raphid diatoms, have the highest proportions during the end of the LGM (10.9%) and early deglacial (Heinrich Stadial 1 [HS1] [9.8%] and Bølling/Allerød [9%]). Their mean proportions decrease continuously until the Mid Holocene (4.7%), but increase again in the Late Holocene (5.5%) (Figure 2).

Constrained hierarchical clustering combined with the broken stick model suggested division into three stratigraphic zones that are consistent with typical climatic phases: the late glacial phase comprising samples dated to 19.91–15.26 cal kyr BP, the deglacial transition phase comprising samples dated to 14.95–10.73 cal kyr BP and the Holocene phase comprising samples dated to 10.43–1.08 cal kyr BP. We therefore used these phases for the description of the *sed*aDNA record.

The glacial phase comprises several ASVs assigned to *Thalassiosira* which account for about 30%–70% of the composition, *Porosira* (9.6%–29.2%), *Chaetoceros* cf. *contortus* 1 SEH 2013 ASV 980 (8.7%–9.6%), *Attheya* ASV 58 (0.4%–6.8%), *Actinocyclus* 1 MPA-2013 (0.9%–5.1%), and *Chaetoceros socialis* ASV 1280 (0.8%–4.7%). Among pennate diatoms, ASVs assigned to *Bacillaria* sp. ASV 139 (0.2%–2.7%), *Navicula ramosissima* ASV 1651 (0%–2.5%), and several *Nitzschia* ASVs have notable proportions.

Although the deglacial phase encompasses climatically very different phases, Cymatosiraceae (0.02%–0.7%) and *Leptocylindrus minimus* (0%–1.4%) ASVs are mostly restricted to this zone. With the onset of this zone, the proportions of most pennate diatoms as well as *Thalassiosira nordenskioeldii* ASV 2697 (mostly <0.1%) decrease. The Bølling/Allerød phase contains ASVs that have their peak proportions during this phase, such as *Paralia* (0.6%–16.8%) and *Thalassiosira* sp. 15BOF (0%–1.2%). While *Thalassiosira angulata* (0.3%–5.2%) and *Nitzschia* cf. *frigida* ASVs 1763 and 1764 (1.3%–4.8%) increase, *C. socialis* ASV 1280 (0%–1.4%) and *Minidiscus trioculatus* (0%–0.8%) show a marked drop during this phase. During the Younger Dryas, some ASVs that decreased during the Bølling/Allerød, increase again, such as *C. socialis* ASV 1280 (3%–5%), *Thalassiosira* sp. ASV 2241 (2.6%–7.4%), and *Attheya* ASV 58 (0%–5.7%).

The Holocene phase is marked by the reduction and sporadic presence of several ASVs assigned to pennate diatoms, yet increased but highly variable proportions of *Haslea avium* (0.02%–4%). Predominantly, the Holocene is composed of sequence types assigned to the genera *Chaetoceros* and *Thalassiosira* as well as *Porosira* (4.4%–33.9%) and *Skeletonema* ASV 2155 (0.3%–10.2%).

3.2. Relationship of Diatom *sed*aDNA Composition With Environmental Variables

We used multivariate statistics to determine to what degree abiotic factors have an effect on the *sed*aDNA composition. June insolation, the sea-ice proxy IP_{25} and the salinity proxy $\delta^{18}O_{ivc\text{-}sw}$ displayed VIF values between 1.003 and 1.009 suggesting low levels of collinearity between each other. Decomposition of the total variance (0.09383) showed that 33.9% of the variance is explained by the model containing the three explanatory variables (adjusted $R^2 = 0.321$). RDA axis 1 captures 22.6% of the variance, while RDA axis 2 captures 11.3%. June insolation is highly correlated with RDA axis 1 (Table 1). Samples located in the right quadrants of the triplot are characterized by high June insolation and mostly centric diatoms of the genera *Chaetoceros*, *Thalassiosira,* and *Skeletonema*. While the upper left quadrant is characterized by high concentrations of the sea-ice biomarker IP_{25}, the lower left quadrant is characterized by heavier $\delta^{18}O_{ivc\text{-}sw}$. Especially in the genus *Chaetoceros*, our data set shows several ASVs assigned to the same species. The RDA triplot shows, for example, that *Chaetoceros socialis* ASV 1280 is located in the upper left quadrant which is associated with late glacial samples and IP_{25} whereas *Chaetoceros socialis* ASV 1281 is located in the lower right quadrant which is associated with Early Holocene samples of the deglacial stratigraphic zone and high June insolation (Figure 4). A second example is shown in the RDA triplot for two ASVs assigned to *Chaetoceros* cf. *pseudobrevis* 1 SHE-2013 with the closest match to the same GenBank accession number (KC985654). While ASV 1143 (98% match with reference) is located in the upper right quadrant and has its highest proportions during the Early Holocene and is strongly reduced since the Mid Holocene (Figure 3), the proportions of ASV 1144 (100% match with reference) increase in the early Mid Holocene and remain on a rather similar level until the Late Holocene.

3.3. Diatom Diversity Changes

Richness (number of ASVs after rarefaction) was lowest in the youngest sample dated to 1.08 cal kyr BP (37 ASVs) and highest about 18.42 cal kyr BP (106 ASVs) (Figures 5 and S1). While the median richness among sequences assigned to centric diatoms varies only slightly over the past 19.9 cal kyr BP, the richness of those assigned to pennate diatoms declines almost continuously throughout the record, except for an increase during the Younger Dryas (Figure S1). The richness of pennate diatom ASVs shows a moderate, positive correlation with IP_{25} ($R^2 = 0.48$, $p = 0.003$), and moderate, negative correlations with June insolation ($R^2 = -0.49$, $p = 0.002$) and NGRIP $\delta^{18}O$ ($R^2 = -0.68$, $p < 0.001$). The richness of centric diatoms does not show any significant correlation with environmental variables Table S1).

Beta-diversity, which is here used as a measure of dissimilarity between adjacent samples, is moderate overall (median = 0.51). There are four strong declines in diatom richness in our record. The first occurred between 18.24 and 18 cal kyr BP and reduced centric diatom ASVs approximately by half (from 62 to 32 ASVs) and pennate ASVs by about a quarter (from 31 to 23 ASVs). Slightly elevated values of beta-diversity (Jaccard dissimilarity = 0.56) during this time in comparison to the median Jaccard dissimilarity correspond more to nestedness rather than turnover (Figure 3). The second decline occurred between 15.6 and 14.24 cal kyr BP and affected pennate diatom ASVs (from 33 to 16 ASVs) more than centric ones (from 49 to 38 ASVs).

Figure 3. Stratigraphic diagram showing the proportions of the assigned amplicon sequence variants for each sample through time. Only sequence variants with more than 1% proportion in one or more samples are shown. If not indicated otherwise, the scales of proportions start with 0%. Centric diatoms are marked in light blue, while pennate diatoms are marked in dark blue, five times exaggeration is shown in gray. The horizontal, dotted lines mark the boundaries of the three CONISS based stratigraphic zones. The CONISS dendrogram and the total sum of squares are given on the right side.

Table 1
Variation Partitioning for the Final Set of Explanatory Variables With Adjusted R^2 and p-Values for the Single and the Individual Fractions (Conditional Variance) Which Remain After Eliminating the Effects of the Remaining Explanatory Variables

		Single		Conditional	
	Variance	Adj. R^2	*p*-value	Adj. R^2	*p*-value
June insolation	0.0116	0.108	0.002	0.040	0.001
IP_{25}	0.0119	0.104	0.002	0.089	0.001
Salinity	0.0113	0.099	0.001	0.023	0.01

Beta-diversity increases from 15.6 to 14.95 cal kyr BP and then slightly decreases again. The third decline affects both pennate and centric diatoms strongly and started after 11.95 until 11.1 cal kyr BP for pennate (from 27 to 6 ASVs) and after 11.42 until 11.1 cal kyr BP for centric diatom ASVs (from 58 to 30 ASVs). Between 11.1 and 10.5 cal kyr BP, the turnover partition of beta-diversity is the highest overall throughout the record. This corresponds predominantly to a loss of ASVs in both pennate and centric diatoms at 11.1 cal kyr BP followed by a gain of ASVs at 10.5 cal kyr BP (Figure 5). The fourth decline is detected between the youngest samples from 1.22 and 1.08 cal kyr BP (from 9 to 6 pennate ASVs and from 53 to 27 centric ASVs) and shows slightly increased beta-diversity, of which the turnover partition is only slightly higher than the nestedness one.

4. Discussion

4.1. General Relationship Between Diatom *sed*aDNA Composition and Environmental Change

4.1.1. Late Glacial Phase (19.9–15.26 cal kyr BP)

The diatom *sed*aDNA composition during the late glacial phase reflects sea ice as a key variable shaping the past diatom communities. The presence of winter sea ice is indicated by sequences assigned to sea ice-associated species such as the colony-forming pennate diatoms *Pauliella taeniata* (Grunow) Round & Basson (Lovejoy et al., 2002; Syvertsen, 1991) and *Nitzschia* cf. *frigida* (Grunow) (Hasle & Heimdal, 1998), or the epiphytic living *Attheya septentrionalis* (Østrup) R.M.Crawford (von Quillfeldt, 1997). These species are frequently detected in modern surveys of sea ice (Limoges et al., 2018; Lovejoy et al., 2002; Poulin et al., 2011; von Quillfeldt, 2000), but can be absent or only sporadically found in surface sediments due to degradation during sinking through the water column (Limoges et al., 2018; Lopes et al., 2006). In such a case, *sed*aDNA has an advantage over assemblage data and can complement the picture we perceive of the past. Winter sea-ice conditions with ice-free summers were also reconstructed based on the sea-ice biomarker IP_{25}

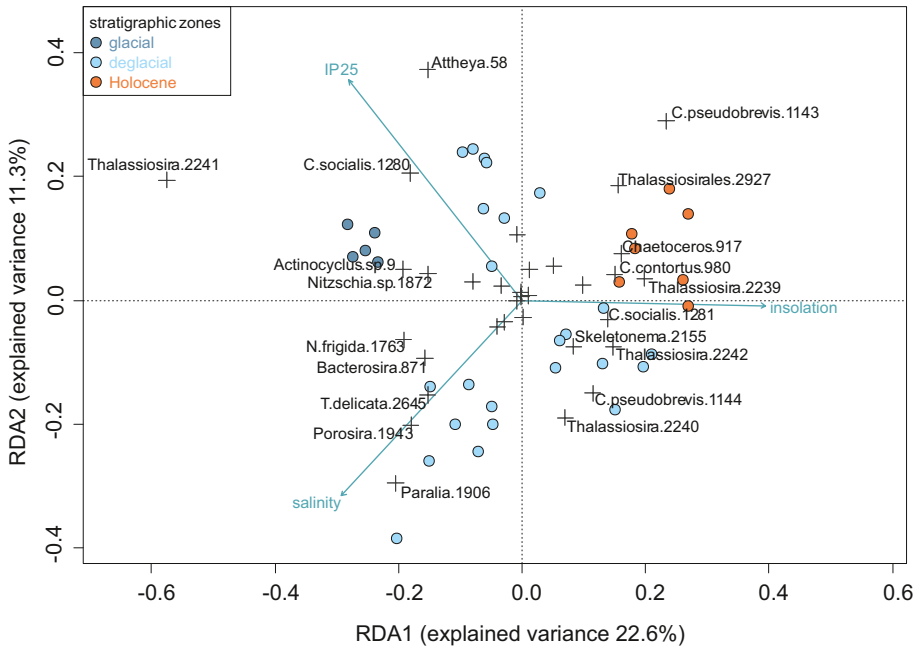

Figure 4. RDA triplot showing the abbreviated names of the 20 most explaining amplicon sequence variants (ASVs) and the vector ends of the most abundant ASVs as a gray plus symbol (+). Samples are marked by color-coded points to the three stratigraphic zones which they represent (dark blue = late glacial, light blue = deglacial, orange = Holocene). Environmental variables are shown by blue vectors.

10.1029/2020PA004091

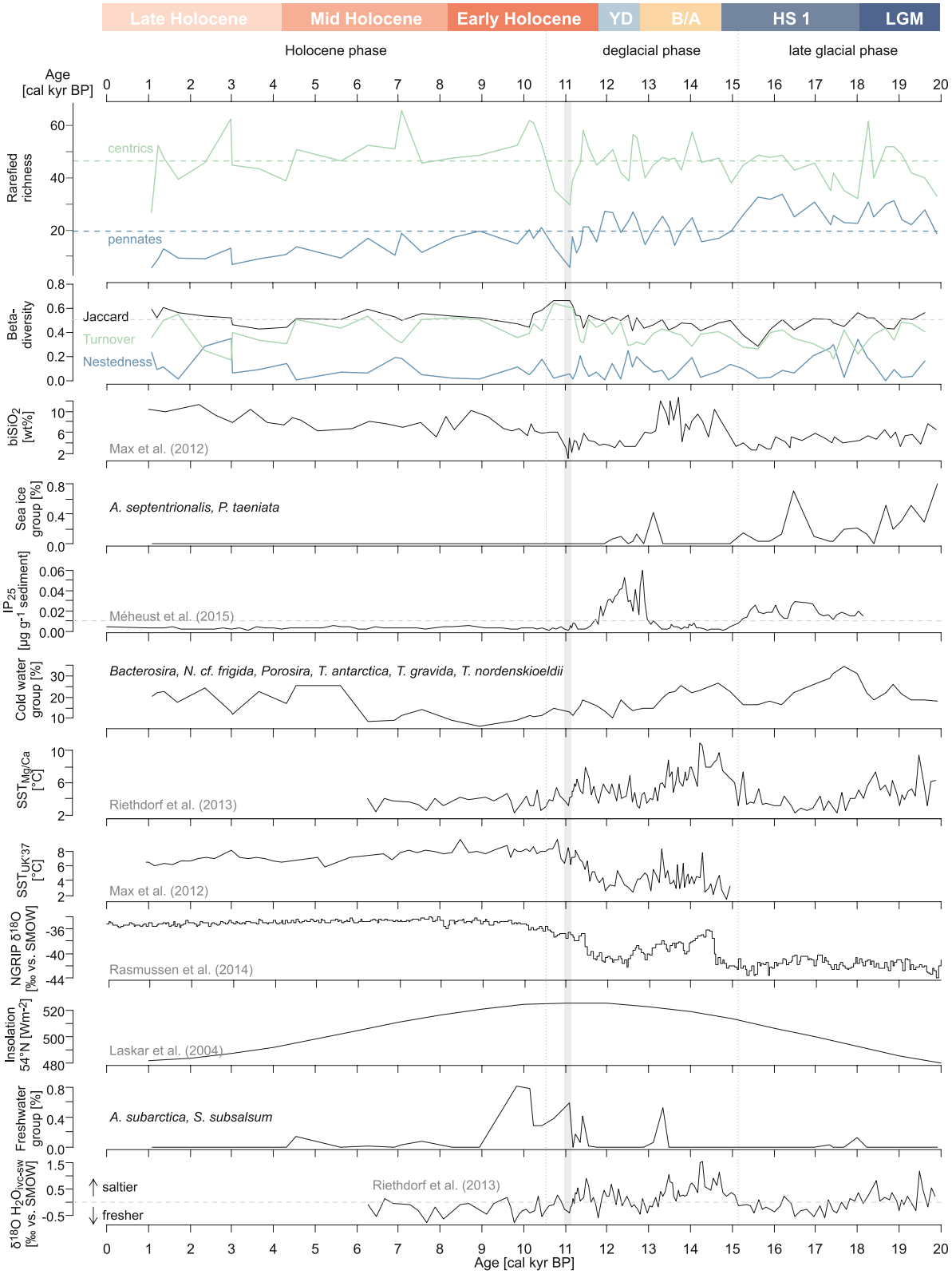

and abundant *Fragilariopsis cylindrus* and *F. oceanica* in local microfossil assemblages (Max et al., 2012a; Méheust et al., 2016; Smirnova et al., 2015). Low proportions of sequences assigned to the productive genus *Chaetoceros* (Lopes et al., 2006) in our record could reflect overall low productivity as also suggested by low biogenic silica (Max et al., 2012a) and low abundance of diatom microfossils during this phase (Smirnova et al., 2015).

The high share of sequences assigned to *Bacterosira*, *T. nordenskioeldii*, *T. antarctica,* and *Porosira* points to ice-free, but cool, summers, although these taxa can also appear in sea ice. Sequences assigned to *Bacterosira* and *Porosira* on genus level likely correspond to *Bacterosira bathyomphala* and *Porosira glacialis* which are common in this region (Ren et al., 2014; Sancetta, 1982). These cold-water species are often found along the winter ice edge in the Bering and Okhotsk Seas and in coastal areas of Kamchatka (Ren et al., 2014), although the neritic species *Bacterosira bathyomphala* could also be associated with shallow slope depths down to 500 m as in the Sea of Okhotsk (Ren et al., 2014; Sancetta, 1982). In the subarctic North Pacific and adjacent seas, these species achieve maximum abundances where summer SSTs remain between 5°C and 8°C, but they can generally be found where summer SSTs remain below 12.5°C (Ren et al., 2014). This is well within the range of previous reconstructions carried out on this sediment core indicating summer SSTs of about 8–9.5°C during this phase (Meyer et al., 2016b). Late glacial diatom microfossil data of this core are characterized by the dominance of the *Thalassiosira trifulta* and *Actinocyclus curvatulus* groups. While our *sed*aDNA reveals much more complexity in the diatom assemblages during this time, our method is still restricted by the incompleteness of the reference database, as, for example, *T. trifulta* and *A. curvatulus* are not available and are potentially only resolved to genus level in our record. Still, *Actinocyclus* sp. 1 MPA-2013 displays higher proportions during the late glacial phase in comparison to the deglacial and Holocene phases, which is in agreement with Smirnova et al. (2015) as well as with microfossil records from Bowers Ridge and the western subarctic gyre (Katsuki & Takahashi, 2005).

Sequences assigned to pennate, raphid diatoms have the highest proportions until approximately 15.7 cal kyr BP, which may be linked to bottom ice communities (Caissie et al., 2010), where they are usually dominant (Poulin et al., 2011; von Quillfeldt, 2000). The benthic lifestyle, to which pennate diatoms are adapted to, includes the excretion of exopolymers via the raphe, which facilitate their attachment to surfaces and enables them to actively move along surfaces such as ice (Olsen et al., 2019; Round et al., 1990). As summer insolation is an important driver for SSTs in the subarctic North Pacific (Harada et al., 2014), it is conceivable that the low summer insolation during this time (Laskar et al., 2004) promoted pennate diatoms due to a long duration of sea-ice coverage with only a short summer. Short-term summers have also been reconstructed during this phase in the Bering Sea, where sea ice was estimated to have covered most of the Bering Sea for more than 6 months (Caissie et al., 2010; Méheust et al., 2016).

4.1.2. Deglacial Transition Phase (14.95–10.73 cal kyr BP)

The *sed*aDNA composition of samples dated to the Bølling/Allerød phase (14.7–12.7 cal kyr BP) can likely be related to increased subsurface salinity in comparison to the glacial phase as implied by an enrichment of $\delta^{18}O_{ivc\text{-}sw}$ (Riethdorf et al., 2013a). Peak proportions of sequences assigned to *Paralia* (*sulcata*) up to ~15% coincide with increasing subsurface salinities (positive $\delta^{18}O_{ivc\text{-}sw}$) during this phase. *Paralia sulcata* (Ehrenberg) Cleve is a coastal species, which is a common part of benthic communities and increased abundance is often recorded in areas of upwelling (Abrantes, 1988; McQuoid & Nordberg, 2003; Stabell, 1986), or where the water column is less stable and subject to strong wind-driven or tidal mixing (McQuoid & Nordberg, 2003).

Sequences assigned to *Thalassiosira delicata*, the cold-water indicator *Porosira*, and *Bacterosira*, but also to the sea-ice associated *Nitzschia* cf. *frigida* suggest a cold-water environment with the frequent influence of

Figure 5. Comparison of rarefied richness (horizontal green dashed line marks median richness of centric diatom ASVs, blue dashed line marks median richness of pennate diatom ASVs), beta-diversity (Jaccard dissimilarity and its partitions into turnover and nestedness), and proportions of diatom *sed*aDNA indicator groups with Mg/Ca-based subsurface SSTs (Riethdorf et al., 2013a), alkenone-based SSTs ($SST_{UK'37}$), biogenic silica (Max et al., 2012a, 2012b), IP_{25} (Méheust et al., 2015), stable oxygen isotopes from Greenland ice cores (NGRIP $\delta^{18}O$; Rasmussen et al., 2014), June insolation calculated after Laskar et al. (2004) and sea subsurface salinity approximation ($\delta^{18}O_{ivc\text{-}sw}$; Riethdorf et al., 2013a). The vertical dotted lines mark the stratigraphic zonation. The shaded vertical area highlights the sample at ~11.1 cal kyr BP.

sea ice despite recorded increases of SSTs by about 3°C–5°C (Max et al., 2012a; Riethdorf et al., 2013a). Such SSTs are still in the growth range of *B. bathyomphala* and *P. glacialis* (Ren et al., 2014). These species also occur in the marginal ice zone, where sea-ice concentration varies between 15% and 80%, and achieve high abundances during the spring bloom (Hasle, 1990). Hence, proportions of sequences assigned to *Nitzschia* cf. *frigida* of more than 3% in this phase are not necessarily contradictory. While the absence of IP_{25} suggests ice-free conditions, gravel-sized ice-rafted debris at about 13.86 cal kyr BP (560 cm depth; Levitan et al., 2015) points toward the presence of sea ice. As *Nitzschia frigida* is a common inhabitant of landfast ice communities (Medlin & Hasle, 1990), a possible explanation could be the occurrence of drifting ice floes, which were transported away from the coast or southward by the East Kamchatka Current, and probably originated from enclosed bights and bays along the eastern coast of Kamchatka (Polyakova, 2007).

The diatom *sed*aDNA composition of samples dated to the Younger Dryas (12.7–11.7 cal kyr BP) is characterized by the presence of sea ice-associated ASVs (*Pauliella taeniata*, *Attheya septentrionalis, Nitzschia* cf. *frigida*) suggesting winter sea-ice coverage during this time. Sea ice-associated ASVs in combination with a higher richness of pennate diatom ASVs in comparison to the Bølling/Allerød phase are in agreement with sea-ice diatom microfossils detected by Smirnova et al. (2015), high concentrations of the sea-ice biomarker IP_{25} (Méheust et al., 2016) and reconstructed subsurface SSTs between about 2°C–5°C with lower seasonal contrasts and a reduced stratification of the mixed layer (Riethdorf et al., 2013a). Upon close inspection, the *sed*aDNA, microfossil, and IP_{25} records show slight differences, that might be explained by different growth optima between species of the *sed*aDNA sea ice group, *Fragilariopsis cylindrus* and *Fragilariopsis oceanica* microfossils and the IP_{25} producers *Haslea spicula*, *Haslea kjellmanii,* and *Pleurosigma stuxbergii* var. *rhomboides* (Brown et al., 2014; Limoges et al., 2018), which highlights the advantage of multiproxy records over the use of a single proxy.

Increased proportions of *Chaetoceros socialis* (ASV 1280) are characteristic in this phase and show comparable proportions with regard to the late glacial phase. This matches the increasing proportions of *Chaetoceros* spp. detected in the microfossil record during this phase (Smirnova et al., 2015). *Chaetoceros socialis* is often dominant in coastal areas with sparse to no sea ice in the Greenland North Water Polynya, where it blooms in late summer; however, it can also achieve substantial abundances in sea ice (Booth et al., 2002; von Quillfeldt, 1997). We therefore assume that this ASV is derived from a lineage adapted to sea ice or marginal ice zone conditions and might represent the novel described *C. gelidus* (Chamnansinp et al., 2013) of which so far no rbcL reference sequence is available. This case shows that for diverse genera such as *Chaetoceros sed*aDNA has the potential to increase taxonomic resolution.

We would like to point out that Smironova et al. (2015) presented the sum of valves of several *Chaetoceros* species. Unfortunately, she did not report how many and which species they were able to determine. Therefore, a comparison between our potential ecotypes and the microfossil record is not possible. The discrepancies between the records of Chaetoceros microfossils and sedaDNA could be a result of preservation bias between the two proxies. While valves get dissolved, the DNA could be released and bind to charged particles, which protects the DNA from degradation by nucleases. As a large fraction of the DNA in subseafloor sediments exists extracellularly (Dell'Anno et al., 2002).

The composition of samples dated to the onset of the Preboreal (11.7–10.73 cal kyr BP) is marked by a decrease in sequences assigned to cold-water diatoms and highest proportions of sequences assigned to freshwater species throughout the record. From about 11.2 cal kyr BP onwards, sequences assigned to *Skeletonema subsalsum* (Cleve-Euler) Bethge and *Aulacoseira subarctica* (Otto Müller) E.Y. Haworth increase strongly. *Skeletonema subsalsum* can be found in rivers, estuaries, and coastal areas (Hasle & Evensen, 1975), while *A. subarctica* is a freshwater species occurring in rivers and turbulent, cool lakes on Kamchatka (Lepskaya et al., 2010). Their increased proportions in the *sed*aDNA record suggest an increased runoff from Kamchatka and possibly contributed to fresher sea-surface conditions in addition to melting sea ice. The timing coincides with the post-glacial opening of the Bering Strait (Jakobsson et al., 2017) and is marked by a high June insolation (Laskar et al., 2004). Fresher subsurface conditions are also indicated by peaks of lighter $\delta^{18}O_{ivc\text{-}sw}$ in this core (Riethdorf et al., 2013a). In a synthesis of $\delta^{18}O$ records from several cores of the Bering Sea and North Pacific region, Gorbarenko et al. (2019) compared a sequence of lighter $\delta^{18}O$ peaks during the Bølling/Allerød with core LV63-41-2 which is located further south of our core and with SO201-2-85KL which is further north in the western Bering Sea. As this sequence was only recorded

in our core, the authors concluded that our study site was influenced by meltwater inputs from Kamchatka glaciers via the Kamchatka River and that southward flowing of the East Kamchatka Current mixed the water masses so that the freshening was not recorded in core LV63-41-2. The record of LV63-41-2 however only contains the phase between the Bølling/Allerød and the LGM, thus such a comparison which would support our inference is not possible for the Early Holocene.

Even though terrestrial soil-derived branched GDGTs and titanium/calcium records of this core suggest overall low terrestrial input, the sum of terrestrial GDGTs peaks during this time (Meyer et al., 2016b, 2017) and might also point toward increased runoff from Kamchatka.

4.1.3. Holocene Phase (10.43–1.08 cal kyr BP)

The *sed*aDNA composition of the Early to Mid Holocene is characterized by reduced proportions of sequences assigned to cold-water species and correlate with high June insolation between ~11 and 6 cal kyr BP (Laskar et al., 2004). The timing fits well into the range of the Holocene Thermal Maximum between ~10 and 8 cal kyr BP (Meyer et al., 2017), with maximum SSTs ranging from 6–11°C ($SST_{UK'37}$) as reconstructed by (Max et al., 2012a) to 10°C–11°C (SST_{TEXL86} August temperatures of Meyer et al., 2016b). During this phase, the proportions of sequences assigned to centric diatoms, especially of the genera *Chaetoceros*, *Thalassiosira* and *Skeletonema*, increase at the expense of sequences assigned to pennate diatoms.

High proportions of *Chaetoceros* are indicative of high productivity, which is supported by increasing biogenic opal (Max et al., 2012a; Riethdorf et al., 2013a) and high diatom microfossil abundances (Smirnova et al., 2015). Sequences assigned as freshwater diatoms and negative $\delta^{18}O_{ivc\text{-}sw}$ values indicate long-term relatively fresh subsurface conditions (Riethdorf et al., 2013a).

From about 6–1 cal kyr BP, increasing proportions of cold-water diatom ASVs reflect cooling, which is in agreement with the climate development recorded in the NGRIP Greenland ice core record (Rasmussen et al., 2014), reconstructed SSTs (Max et al., 2012a; Meyer et al., 2016b, 2017; Riethdorf et al., 2013a) and the advance of glaciers on Kamchatka (between 4.5 and 3.5 cal kyr BP) (Brooks et al., 2015). A drop in cold-water diatoms at ~3 cal kyr BP, suggests a short-term interruption of this phase of cooling, which is synchronous with a short-term increase of $SST_{UK'37}$ (Max et al., 2012).

An increase of sequences assigned to pennate diatoms in the Late Holocene and high proportions of cold-water diatom ASVs including the ice-associated *Nitzschia* cf. *frigida* suggest cooling and potentially an increasing influence of winter sea ice or at least drifting ice floes in the region. In support of this, grain-size analyses of this core suggest increased presence of potentially ice-rafted material (Levitan et al., 2015) and after 6 cal kyr BP the microfossil assemblage contains sea ice-associated species (Smirnova et al., 2015), whereas the sea-ice biomarker IP_{25} suggests ice-free conditions (Méheust et al., 2016). Thus, *sed*aDNA has the potential to complement our understanding of past sea-ice distribution.

4.2. Changes in Diatom *sed*aDNA Richness and the Relationship With Environmental Changes

Richness of pennate diatom ASVs was higher during phases of strong Northern Hemisphere cooling, namely the late LGM, Heinrich Stadial 1, and the Younger Dryas, and is significantly positively correlated with sea ice and significantly negatively correlated with June insolation and Northern Hemisphere temperatures. This points toward sea ice as a facilitating factor for pennate diatoms with regard to alpha-diversity in the subarctic NW Pacific. The negative correlation of pennate diatom richness with June insolation and temperatures in comparison to centric diatom richness might be related to the higher sensitivity of pennate diatoms to ultraviolet light in the absence of a thick sea-ice cover, whereas centric diatoms have developed strategies to prevent damage to their photosystems (Enberg et al., 2015).

A strong decline of richness accompanied by increased beta-diversity occurred during the Preboreal phase of the Early Holocene around 11.1 cal kyr BP and could be attributed predominantly to turnover by loss of ASVs until 11.1 cal kyr BP and replacement by different ASVs of both similar and different species/genera toward 10.5 cal kyr BP. This decline of richness occurs simultaneously with a sharp drop in biogenic opal, suggesting strongly reduced productivity of siliceous organisms such as diatoms (Max et al., 2012a). This interval is characterized by a peak in summer insolation, rising SSTs (Max et al., 2012a) and strong sea-level rise which culminated in the opening of the Bering Strait (Jakobsson et al., 2017). A sharp increase in

proportions of the freshwater group and negative $\delta^{18}O_{ivc\text{-}sw}$ points toward increased sea-surface freshening, potentially derived from increased runoff from Kamchatka (Gorbarenko et al., 2019; Riethdorf et al., 2013a) as suggested by a peak in terrestrial lipid biomarkers around 11.2 cal kyr BP (Meyer et al., 2016b, 2017). Fresher surface conditions could have resulted in enhanced vertical stratification limiting the mixing of nutrients from deeper water masses toward the euphotic zone and thus restricting primary productivity, manifested as a sharp drop of biogenic silica during this time (Max et al., 2012).

Copy number variation may influence richness estimates, as the chance of long-term preservation of the rbcL gene is higher, when more copies are available per cell. This could have an effect on the presence/absence especially of rare taxa, with only one or a few chloroplasts per cell. Yet, our rarefaction curves (Figure S3) are close to saturation which suggests, that it is unlikely, that missing taxa would bias the overall richness patterns in such a way that it would change our conclusions.

With *sed*aDNA, the genus *Chaetoceros* was detected continuously with a variety of species, including known cryptic species pairs from the Bay of Fundy (e.g., *C. decipiens* and *C. diadema*) which appear to have seasonally different distributions (Hamsher et al., 2013). In several cases, different ASVs which were assigned to the same species simply co-occurred while a few, such as *C. pseudobrevis* showed turnover patterns consistent with changes in environmental conditions (ASV 1143 had higher proportions during the Holocene thermal optimum phase, and was almost replaced by ASV 1144 after 7 cal kyr BP), which supports that different ASV are potentially derived from different lineages adapted to different growth conditions (Hamsher et al., 2013). This emphasizes the value of (paleo-)genetic data, as such information would go undetected in microfossil assemblages, especially, as valves of *Chaetoceros* are prone to dissolution and might not be preserved. When we know more about the biogeography and environmental preferences of these variants (e.g., nutrient limitation, temperature constraints), their presence in *sed*aDNA records could help to reconstruct past seasonal environmental conditions. This is supported by a recent study in which ASVs of the foraminifer *N. pachyderma* were traced in a 140,000-year spanning *sed*aDNA record and correlated with oceanographic changes (Pawłowska, Łącka, et al., 2020; Pawłowska, Wollenburg, et al., 2020). This is further proof of the potential of *sed*aDNA to trace responses of microbial eukaryotes to environmental changes on population level (Pawłowska, Łącka, et al., 2020; Pawłowska, Wollenburg, et al., 2020).

The co-occurrence of several ASVs that could not be attributed to environmental changes might have escaped our filter approach and could be a result of the degraded state of ancient DNA that can introduce erroneous nucleotides during PCR (Hofreiter et al., 2001). Alternatively, they could be true variants, which, according to the standing variation hypothesis, allow species to quickly adapt to changing environmental conditions (Godhe & Rynearson, 2017). The application of ASVs, in comparison to clustering into operational taxonomic units, thus has the advantage of revealing (pseudo-)cryptic species or ecotypes and should be considered more in biogeographic surveys.

Diatoms have been shown to impact marine plankton structure by biotic interactions, for example, by competition or selective grazing (Vincent & Bowler, 2020) and exopolymers excreted by sea-ice diatoms have been shown to be hotspots for enhanced bacterial activity (Meiners et al., 2008). Hence, the detected changes could substantially impact marine food-webs and biogeochemical cycling. To what extent changes in the diversity and composition of past diatom assemblages affected the past organismal community at the ecosystem level remains to be revealed, for example, by metagenomic shotgun sequencing of *sed*aDNA approaches.

5. Conclusions

We present the first diatom-derived *sed*aDNA metabarcoding record of the subarctic NW Pacific, which covers the past 19.9 cal kyr.

The dominant components of the diatom *sed*aDNA composition fit well within the framework of reconstructed sea-ice dynamics, SSTs, and subsurface salinities over the past millennia. High proportions of sea-ice and cold-water associated diatoms and generally high proportions of pennate diatoms point to sea ice as the main driver of diatom composition during the late glacial phase as well as during the Younger Dryas. A

positive correlation of pennate diatom richness with the sea-ice biomarker IP_{25} suggests that an extended winter sea-ice cover during the late glacial and the Younger Dryas potentially acted as a diversifying force.

Substantial proportions of *Nitzschia* cf. *frigida* in the absence of the sea-ice proxy IP_{25} during the early deglacial phase point to a continued influence of drifting sea ice. This suggests either that the ecology of *N. frigida* is not completely understood yet, or that our proxy can occasionally be more sensitive to the past presence of sea ice than IP_{25}.

Unfavorable conditions for pennate diatoms at the start of the Holocene are suggested by decreasing proportions and the negative correlation of pennate diatom richness with June insolation and temperature.

The inferred loss of 42% of diatom ASVs at ~11.1 cal kyr BP is accompanied by freshwater diatoms implying the influence of runoff from Kamchatka to the local assemblage. It is likely that the freshwater input resulted in enhanced vertical stratification limiting the mixing of nutrients from deeper water masses toward the euphotic zone and thus restricting primary productivity—a scenario which is supported by near-zero biogenic silica during this time. As modern climate warming is anticipated to increase freshwater input into the Arctic from 11% to 30% by river discharge alone (Nummelin et al., 2016), an enhanced stratification with restricted nutrient supply could have tremendous consequences for the biological carbon pump, biogeochemical cycling and the food-web in the Arctic.

Finally, our proxy revealed shifts of potential ecotypes of species from the genus *Chaetoceros,* which is in agreement with the concept that intra-specific variation facilitates an adaptive response to changing environmental conditions and is particularly relevant in high-latitudinal ecosystems. Therefore, marine *sed*aDNA has the potential to answer ecological questions regarding selective or adaptive responses at an intra-specific level where microfossil studies might be severely limited.

Conflict of Interests

The authors declare that there are no conflict of interests.

Data Availability Statement

Data sets for this study are available in Dryad (H. H. Zimmermann, Stoof-Leichsenring, Kruse, Nuernberg, et al., 2020; H. H. Zimmermann, Stoof-Leichsenring, Kruse, Müller, et al., 2020). The rarefaction script is available at https://github.com/StefanKruse/R_Rarefaction (Kruse, 2019).

Acknowledgments
The authors thank Sarah Olischläger and Iris Eder for support with the laboratory work, Lars Max for providing the age-depth model, Cathy Jenks for English correction, and the captain and crew of the RV Sonne. The KALMAR Project (SO201-2- KALMAR Leg 2) was funded by the Federal German Ministry of Education and Research (BMBF). Open access funding enabled and organized by Projekt DEAL.

References

Abrantes, F. (1988). Diatom assemblages as upwelling indicators in surface sediments off Portugal. *Marine Geology*, *85*(1), 15–39. https://doi.org/10.1016/0025-3227(88)90082-5

Baselga, A., & Orme, C. D. L. (2012). betapart: An R package for the study of beta diversity. *Methods in Ecology and Evolution*, *3*(5), 808–812. https://doi.org/10.1111/j.2041-210X.2012.00224.x

Binladen, J., Gilbert, M. T. P., Bollback, J. P., Panitz, F., Bendixen, C., Nielsen, R., & Willerslev, E. (2007). The use of coded PCR primers enables high-throughput sequencing of multiple homolog amplification products by 454 parallel sequencing. *PLoS ONE*, *2*(2), e197. https://doi.org/10.1371/journal.pone.0000197

Booth, B. C., Larouche, P., Bélanger, S., Klein, B., Amiel, D., & Mei, Z.-P. (2002). Dynamics of *Chaetoceros socialis* blooms in the North Water. *Deep Sea Research Part II: Topical Studies in Oceanography*, *49*(22), 5003–5025. https://doi.org/10.1016/S0967-0645(02)00175-3

Boyer, F., Mercier, C., Bonin, A., Le Bras, Y., Taberlet, P., & Coissac, E. (2016). obitools: Aunix-inspired software package for DNA metabarcoding. *Molecular Ecology Resources*, *16*, 176–182. https://doi.org/10.1111/1755-0998.12428

Brooks, S. J., Diekmann, B., Jones, V. J., & Hammarlund, D. (2015). Holocene environmental change in Kamchatka: A synopsis. *Global and Planetary Change*, *134*, 166–174. https://doi.org/10.1016/j.gloplacha.2015.09.004

Brown, T. A., Belt, S. T., Tatarek, A., & Mundy, C. J. (2014). Source identification of the Arctic sea ice proxy IP_{25}. *Nature Communications*, *5*, 4197. https://doi.org/10.1038/ncomms5197

Caissie, B. E., Brigham-Grette, J., Lawrence, K. T., Herbert, T. D., & Cook, M. S. (2010). Last Glacial Maximum to Holocene sea surface conditions at Umnak Plateau, Bering Sea, as inferred from diatom, alkenone, and stable isotope records. *Paleoceanography*, *25*(1). https://doi.org/10.1029/2008PA001671

Callahan, B. J., McMurdie, P. J., & Holmes, S. P. (2017). Exact sequence variants should replace operational taxonomic units in marker-gene data analysis. *The ISME Journal*, *11*(12), 2639–2643. https://doi.org/10.1038/ismej.2017.119

Chamnansinp, A., Li, Y., Lundholm, N., & Moestrup, Ø. (2013). Global diversity of two widespread, colony-forming diatoms of the marine plankton, *Chaetoceros socialis* (syn. *C. radians*) and *Chaetoceros gelidus* sp. nov. *Journal of Phycology*, *49*(6), 1128–1141. https://doi.org/10.1111/jpy.12121

Corinaldesi, C., Beolchini, F., & Dell'Anno, A. (2008). Damage and degradation rates of extracellular DNA in marine sediments: Implications for the preservation of gene sequences. *Molecular Ecology*, *17*(17), 3939–3951. https://doi.org/10.1111/j.1365-294X.2008.03880.x

Coupel, P., Ruiz-Pino, D., Sicre, M. A., Chen, J. F., Lee, S. H., Schiffrine, N., et al. (2015). The impact of freshening on phytoplankton production in the Pacific Arctic Ocean. *Progress in Oceanography*, *131*, 113–125. https://doi.org/10.1016/j.pocean.2014.12.003

De Schepper, S., Ray, J. L., Skaar, K. S., Sadatzki, H., Ijaz, U. Z., Stein, R., & Larsen, A. (2019). The potential of sedimentary ancient DNA for reconstructing past sea ice evolution. *The ISME Journal*, *13*, 2566–2577. https://doi.org/10.1038/s41396-019-0457-1

Degerlund, M., Huseby, S., Zingone, A., Sarno, D., & Landfald, B. (2012). Functional diversity in cryptic species of *Chaetoceros socialis* Lauder (Bacillariophyceae). *Journal of Plankton Research*, *34*(5), 416–431. https://doi.org/10.1093/plankt/fbs004

Dell'Anno, A., Stefano, B., & Danovaro, R. (2002). Quantification, base composition, and fate of extracellular DNA in marine sediments. *Limnology & Oceanography*, *47*(3), 899–905. https://doi.org/10.4319/lo.2002.47.3.0899

Dulias, K., Stoof-Leichsenring, K. R., Pestryakova, L. A., & Herzschuh, U. (2017). Sedimentary DNA versus morphology in the analysis of diatom-environment relationships. *Journal of Paleolimnology*, *57*(1), 51–66. https://doi.org/10.1007/s10933-016-9926-y

Enberg, S., Piiparinen, J., Majaneva, M., Vähätalo, A. V., Autio, R., & Rintala, J.-M. (2015). Solar PAR and UVR modify the community composition and photosynthetic activity of sea ice algae. *FEMS Microbiology Ecology*, *91*(10). https://doi.org/10.1093/femsec/fiv102

Epp, L. S., Zimmermann, H. H., & Stoof-Leichsenring, K. R. (2019). Sampling and extraction of ancient DNA from sediments. In B. Shapiro, A. Barlow, P. D. Heintzman, M. Hofreiter, J. L. A. Paijmans, & A. E. R. Soares, (Eds.), *Ancient DNA: Methods and protocols* (pp. 31–44). Springer New York. https://doi.org/10.1007/978-1-4939-9176-1_5

Fetterer, F., Knowles, K., Meier, W. N., Savoie, M., & Windnagel, A. K. (2017). *Sea Ice Index, Version 3. Monthly and daily GIS compatible shapefiles of median ice extent [Data set]*. National Snow and Ice Data Center. https://doi.org/10.7265/n5k072f8

Gebhardt, H., Sarnthein, M., Grootes, P. M., Kiefer, T., Kuehn, H., Schmieder, F., & Röhl, U. (2008). Paleonutrient and productivity records from the subarctic North Pacific for Pleistocene glacial terminations I to V. *Paleoceanography*, *23*(4). https://doi.org/10.1029/2007PA001513

Gilbert, M. T. P., Hansen, A. J., Willerslev, E., Rudbeck, L., Barnes, I., Lynnerup, N., & Cooper, A. (2003). Characterization of genetic miscoding lesions caused by postmortem damage. *The American Journal of Human Genetics*, *72*(1), 48–61. https://doi.org/10.1086/345379

Godhe, A., & Rynearson, T. (2017). The role of intraspecific variation in the ecological and evolutionary success of diatoms in changing environments. *Philosophical Transactions of the Royal Society B: Biological Sciences*, *372*(1728), 20160399. https://doi.org/10.1098/rstb.2016.0399

Gorbarenko, S., Shi, X., Zou, J., Velivetskaya, T., Artemova, A., Liu, Y., et al. (2019). Evidence of meltwater pulses into the North Pacific over the last 20 ka due to the decay of Kamchatka Glaciers and Cordilleran Ice Sheet. *Global and Planetary Change*, *172*, 33–44. https://doi.org/10.1016/j.gloplacha.2018.09.014

Grimm, E. C. (1987). CONISS: A FORTRAN 77 program for stratigraphically constrained cluster analysis by the method of incremental sum of squares. *Computers & Geosciences*, *13*(I), 13–35. https://doi.org/10.1016/0098-3004(87)90022-7

Hamsher, S. E., LeGresley, M. M., Martin, J. L., & Saunders, G. W. (2013). A comparison of morphological and molecular-based surveys to estimate the species richness of *Chaetoceros* and *Thalassiosira* (Bacillariophyta), in the Bay of Fundy. *PLoS ONE*, *8*(10), e73521. https://doi.org/10.1371/journal.pone.0073521

Harada, N., Katsuki, K., Nakagawa, M., Matsumoto, A., Seki, O., Addison, J. A., et al. (2014). Holocene sea surface temperature and sea ice extent in the Okhotsk and Bering Seas. *Progress in Oceanography*, *126*, 242–253. https://doi.org/10.1016/j.pocean.2014.04.017

Harrell, F. E., Jr. (2020). *Hmisc: Harrell miscellaneous. R package version 4.4-0*. Retrieved from https://CRAN.R-project.org/package=Hmisc

Hasle, G. R. (1990). Arctic plankton diatoms: Dominant species, biogeography. In L. K. Medlin, & J. Priddle, (Eds.), *Polar marine diatoms* (pp. 53–56). British Antarctic Survey, Natural Environment Research Council.

Hasle, G. R., & Evensen, D. L. (1975). Brackish-water and fresh-water species of the diatom genus *Skeletonema* Grev. I. *Skeletonema subsalsum* (A. Cleve) Bethge. *Phycologia*, *14*(4), 283–297. https://doi.org/10.2216/i0031-8884-14-4-283.1

Hasle, G. R., & Heimdal, B. R. (1998). The net phytoplankton in Kongsfjorden, Svalbard, July 1988, with general remarks on species composition of Arctic phytoplankton. *Polar Research*, *17*(1), 31–52. https://doi.org/10.3402/polar.v17i1.6605

Hofreiter, M., Jaenicke, V., Serre, D., Haeseler, A., & Pääbo, S. (2001). DNA sequences from multiple amplifications reveal artifacts induced by cytosine deamination in ancient DNA. *Nucleic Acids Research*, *29*. https://doi.org/10.1093/nar/29.23.4793

Hsieh, T. C., Ma, K. H., & Chao, A. (2016). iNEXT: An R package for rarefaction and extrapolation of species diversity (Hill numbers). *Methods in Ecology and Evolution*, *7*(12), 1451–1456. https://doi.org/10.1111/2041-210X.12613

Huang, S., Herzschuh, U., Pestryakova, L. A., Zimmermann, H. H., Davydova, P., Biskaborn, B. K., et al. (2020). Genetic and morphologic determination of diatom community composition in surface sediments from glacial and thermokarst lakes in the Siberian Arctic. *Journal of Paleolimnology*. *64*, 225–242. https://doi.org/10.1007/s10933-020-00133-1

Jakobsson, M., Pearce, C., Cronin, T. M., Backman, J., Anderson, L. G., Barrientos, N., et al. (2017). Post-glacial flooding of the Bering Land Bridge dated to 11 cal ka BP based on new geophysical and sediment records. *Climate of the Past*, *13*(8), 991–1005. https://doi.org/10.5194/cp-13-991-2017

Juggins, S. (2012). *rioja: Analysis of quaternary science data, R package version 0*.

Kanz, C., Aldebert, P., Althorpe, N., Baker, W., Baldwin, A., Bates, K., et al. (2005). The EMBL nucleotide sequence database. *Nucleic Acids Research*, *33*(Database Issue), 29–33. https://doi.org/10.1093/nar/gki098

Katsuki, K., & Takahashi, K. (2005). Diatoms as paleoenvironmental proxies for seasonal productivity, sea-ice and surface circulation in the Bering Sea during the late Quaternary. *Deep Sea Research Part II: Topical Studies in Oceanography*, *52*(16), 2110–2130. https://doi.org/10.1016/j.dsr2.2005.07.001

Kruse, S. (2019). *R code for resampling and thus normalizing of count data to the minimum number of counts across a set of samples (e.g. sedaDNA sequence/pollen taxa counts per sample along a sediment core)*. Retrieved from https://github.com/StefanKruse/R_Rarefaction

Laskar, J., Robutel, P., Joutel, F., Gastineau, M., Correia, A. C. M., & Levrard, B. (2004). A long-term numerical solution for the insolation quantities of the Earth. *Astronomy & Astrophysics*, *428*, 261–285. https://doi.org/10.1051/0004-6361:20041335

Lepskaya, E. V., Jewson, D. H., & Usoltseva, M. V. (2010). Aulacoseira subarcticain Kurilskoye Lake, Kamchatka: A deep, oligotrophic lake and important Pacific salmon nursery. *Diatom Research*,*25*(2), 323–335. https://doi.org/10.1080/0269249X.2010.9705853

Levitan, M. A., Kuz'mina, T. G.,Luksha, V. L.,Roshchina, I. A., Syromyatnikov, K. V., Max, L., et al. (2015). Evolution of sedimentation on the continental slope of the Kronotskii Peninsula (Eastern Kamchatka) over the last 20 ka. *Lithology and Mineral Resources*, *50*(4), 249–269. https://doi.org/10.1134/S0024490215040045

Li, W. K. W., McLaughlin, F. A., Lovejoy, C., & Carmack, E. C. (2009). Smallest algae thrive as the Arctic Ocean freshens. *Science*, *326*(5952), 539. https://doi.org/10.1126/science.1179798

Limoges, A., Massé, G., Weckström, K., Poulin, M., Ellegaard, M., Heikkilä, M., et al. (2018). Spring succession and vertical export of diatoms and IP_{25} in a seasonally ice-covered high Arctic fjord. *Frontiers of Earth Science*, *6*. https://doi.org/10.3389/feart.2018.00226

Lopes, C., Mix, A. C., & Abrantes, F. (2006). Diatoms in northeast Pacific surface sediments as paleoceanographic proxies. *Marine Micropaleontology*, *60*(1), 45–65. https://doi.org/10.1016/j.marmicro.2006.02.010

Lovejoy, C., Legendre, L., Martineau, M.-J., Bâcle, J., & von Quillfeldt, C. H. (2002). Distribution of phytoplankton and other protists in the North Water. *Deep Sea Research Part II: Topical Studies in Oceanography*, *49*(22), 5027–5047. https://doi.org/10.1016/S0967-0645(02)00176-5

Matul', A. G., Saidova, K M., Smirnova, M. A., Khusid, T. A., Kazarina, G. K., & Chekhovskaya, M. P. (2015). Rapid diachronous paleoceanographic changes in the Far East marginal areas of the Pacific Ocean at the last glaciation-to-holocene transition. *Doklady Earth Sciences*, *463*(2), 873–877. https://doi.org/10.1134/S1028334X1508022X

Max, L., Riethdorf, J.-R., Tiedemann, R., Smirnova, M., Lembke-Jene, L., Fahl, K., et al. (2012a). *Biogenic opal of sediment core SO201-2-12 [Data set]*. PANGAEA. https://doi.org/10.1594/PANGAEA.786197

Max, L., Riethdorf, J.-R., Tiedemann, R., Smirnova, M., Lembke-Jene, L., Fahl, K., et al. (2012b). Sea surface temperature variability and sea-ice extent in the subarctic northwest Pacific during the past 15,000 years. *Paleoceanography*, *27*(3). https://doi.org/10.1029/2012PA002292

McQuoid, M. R., & Nordberg, K. (2003). The diatom Paralia sulcata as an environmental indicator species in coastal sediments. *Estuarine, Coastal and Shelf Science*, *56*(2), 339–354. https://doi.org/10.1016/S0272-7714(02)00187-7

Medlin, L. K., & Hasle, G. R. (1990). Some *Nitzschia* and related diatom species from fast ice samples in the Arctic and Antarctic. *Polar Biology*, *10*(6). https://doi.org/10.1007/BF00233693

Méheust, M., Stein, R., Fahl, K., Max, L., & Riethdorf, J.-R. (2015). *High-resolution IP25 of sediment core SO201-2-12 [Data set]*. PANGAEA. https://doi.org/10.1594/PANGAEA.855451

Méheust, M., Stein, R., Fahl, K., Max, L., & Riethdorf, J.-R. (2016). High-resolution IP25-based reconstruction of sea-ice variability in the western North Pacific and Bering Sea during the past 18,000 years. *Geo-Marine Letters*, *36*(2), 101–111. https://doi.org/10.1007/s00367-015-0432-4

Meiners, K., Krembs, C., & Gradinger, R. (2008). Exopolymer particles: Microbial hotspots of enhanced bacterial activity in Arctic fast ice (Chukchi Sea). *Aquatic Microbial Ecology*, *52*(2), 195–207. https://doi.org/10.3354/ame01214

Meyer, V. D., Hefter, J., Lohmann, G., Max, L., Tiedemann, R., & Mollenhauer, G. (2017). Summer temperature evolution on the Kamchatka Peninsula, Russian Far East, during the past 20 000 years. *Climate of the Past*, *13*(4), 359–377. https://doi.org/10.5194/cp-13-359-2017

Meyer, V. D., Max, L., Hefter, J., Tiedemann, R., & Mollenhauer, G. (2016a). *Fractional abundances of isoprenoid and branched glycerol dialkyl glycerol tetraethers (GDGT) of sediment core SO201-2-12KL [Data set]*. PANGAEA. https://doi.org/10.1594/PANGAEA.862964

Meyer, V. D., Max, L., Hefter, J., Tiedemann, R., & Mollenhauer, G. (2016b). Glacial-to-Holocene evolution of sea surface temperature and surface circulation in the subarctic northwest Pacific and the Western Bering Sea. *Paleoceanography*, *31*(7), 916–927. https://doi.org/10.1002/2015PA002877

Nagano, A., Wakita, M., & Watanabe, S. (2016). Dichothermal layer deepening in relation with halocline depth change associated with northward shrinkage of North Pacific western subarctic gyre in early 2000s. *Ocean Dynamics*, *66*(2), 163–172. https://doi.org/10.1007/s10236-015-0917-8

Nummelin, A., Ilicak, M., Li, C., & Smedsrud, L. H. (2016). Consequences of future increased Arctic runoff on Arctic Ocean stratification, circulation, and sea ice cover. *Journal of Geophysical Research: Oceans*, *121*(1), 617–637. https://doi.org/10.1002/2015JC011156

Oksanen, J., Blanchet, F. G., Kindt, R., Legendre, P., Minchin, P. R., O'Hara, R. B., et al. (2011). *vegan: Community ecology package. R package version 2.0-2*.

Olsen, L. M., Duarte, P., Peralta-Ferriz, C., Kauko, H. M., Johansson, M., Peeken, I., et al. (2019). A red tide in the pack ice of the Arctic Ocean. *Scientific Reports*, *9*. https://doi.org/10.1038/s41598-019-45935-0

Pääbo, S. (1989). Ancient DNA: Extraction, characterization, molecular cloning, and enzymatic amplification. *Proceedings of the National Academy of Sciences of the United States of America*, *86*(6), 1939–1943. https://doi.org/10.1073/pnas.86.6.1939

Parkinson, C. L., Cavalieri, D. J., Gloersen, P., Zwally, H. J., & Comiso, J. C. (1999). Arctic sea ice extents, areas, and trends, 1978-1996. *Journal of Geophysical Research*, *104*(C9), 20837–20856. https://doi.org/10.1029/1999JC900082

Pawłowska, J., Łącka, M., Kucharska, M., Pawlowski, J., & Zajączkowski, M. (2020). Multiproxy evidence of the Neoglacial expansion of Atlantic Water to eastern Svalbard. *Climate of the Past*, *16*(2), 487–501. https://doi.org/10.5194/cp-16-487-2020

Pawłowska, J., Wollenburg, J. E., Zajączkowski, M., & Pawlowski, J. (2020). Planktonic foraminifera genomic variations reflect paleoceanographic changes in the Arctic: evidence from sedimentary ancient DNA. *Scientific Reports*, *10*(1), 15102. https://doi.org/10.1038/s41598-020-72146-9

Pistone, K., Eisenman, I., & Ramanathan, V. (2014). Observational determination of albedo decrease caused by vanishing Arctic sea ice. *Proceedings of the National Academy of Sciences of the United States of America*, *111*(9), 3322–3326. https://doi.org/10.1073/pnas.1318201111

Polyakova, A. M. (2007). Extreme supply of floating ice to the northwestern part of the Pacific Ocean. *Oceanology*, *47*(1), 1–4. https://doi.org/10.1134/S0001437007010018

Poulin, M., Daugbjerg, N., Gradinger, R., Ilyash, L., Ratkova, T., & von Quillfeldt, C. (2011). The pan-Arctic biodiversity of marine pelagic and sea-ice unicellular eukaryotes: A first-attempt assessment. *Marine Biodiversity*, *41*(1), 13–28. https://doi.org/10.1007/s12526-010-0058-8

R Core Team. (2018). *R: A language and environment for statistical computing*. R Foundation for Statistical Computing. Retrieved from https://www.R-project.org/

Rasmussen, S. O., Bigler, M., Blockley, S. P., Blunier, T., Buchardt, S. L., Clausen, H. B., et al. (2014). A stratigraphic framework for abrupt climatic changes during the Last Glacial period based on three synchronized Greenland ice-core records: refining and extending the INTIMATE event stratigraphy. *Quaternary Science Reviews*, *106*, 14–28. https://doi.org/10.1016/j.quascirev.2014.09.007

Ren, J., Gersonde, R., Esper, O., & Sancetta, C. (2014). Diatom distributions in northern North Pacific surface sediments and their relationship to modern environmental variables. *Palaeogeography, Palaeoclimatology, Palaeoecology*, *402*, 81–103. https://doi.org/10.1016/j.palaeo.2014.03.008

Ren, J., Jiang, H., Seidenkrantz, M.-S., & Kuijpers, A. (2009). A diatom-based reconstruction of Early Holocene hydrographic and climatic change in a southwest Greenland fjord. *Marine Micropaleontology*, *70*(3–4), 166–176. https://doi.org/10.1016/j.marmicro.2008.12.003

Reschke, M., Kunz, T., & Laepple, T. (2019). Comparing methods for analysing time scale dependent correlations in irregularly sampled time series data. *Computers & Geosciences*, *123*, 65–72. https://doi.org/10.1016/j.cageo.2018.11.009

Riethdorf, J.-R., Max, L., Nürnberg, D., Lembke-Jene, L., & Tiedemann, R. (2013a). Deglacial development of (sub) sea surface temperature and salinity in the subarctic northwest Pacific: Implications for upper-ocean stratification. *Paleoceanography*, *28*(1), 91–104. https://doi.org/10.1002/palo.20014

Riethdorf, J.-R., Max, L., Nürnberg, D., Lembke-Jene, L., & Tiedemann, R. (2013b). *Stable isotopes measured on benthic foraminifers of sediment core SO201-2-12 [Data set]*. PANGAEA. https://doi.org/10.1594/PANGAEA.786246

Rimet, F., Gusev, E., Kahlert, M., Kelly, M. G., Kulikovskiy, M., Maltsev, Y., et al. (2019). Diat.barcode, an open-access curated barcode library for diatoms. *Scientific Reports*, *9*(1). 15116. https://doi.org/10.1038/s41598-019-51500-6

Rotatore, C., Colman, B., & Kuzma, M. (1995). The active uptake of carbon dioxide by the marine diatoms *Phaeodactylum ticornutum* and *Cyclotella* sp. *Plant, Cell and Environment*, *18*(8), 913–918. https://doi.org/10.1111/j.1365-3040.1995.tb00600.x

Round, F. E., Crawford, R. M., & Mann, D. G. (1990). *Diatoms: Biology and morphology of the genera*. Cambridge University Press.

Sancetta, C. (1979). Oceanography of the North Pacific during the last 18,000 years: Evidence from fossil diatoms. *Marine Micropaleontology*, *4*, 103–123. https://doi.org/10.1016/0377-8398(79)90009-4

Sancetta, C. (1982). Distribution of diatom species in surface sediments of the Bering and Okhotsk Seas. *Micropaleontology*, *28*(3), 221–257. https://doi.org/10.2307/1485181

Sancetta, C., & Silvestri, S. (1986). Pliocene-Pleistocene evolution of the North Pacific Ocean-Atmosphere system, interpreted from fossil diatoms. *Paleoceanography*, *1*(2), 163–180. https://doi.org/10.1029/PA001i002p00163

Schlitzer, R. (2002). Interactive analysis and visualization of geoscience data with Ocean Data View. *Computers & Geosciences*, *28*(10), 1211–1218. https://doi.org/10.1016/S0098-3004(02)00040-7

Schnell, I. B., Bohmann, K., & Gilbert, M. T. P. (2015). Tag jumps illuminated – Reducing sequence-to-sample misidentifications in metabarcoding studies. *Molecular Ecology Resources*, *15*(6), 1289–1303. https://doi.org/10.1111/1755-0998.12402

Shu, Q., Qiao, F., Song, Z., Zhao, J., & Li, X. (2018). Projected freshening of the Arctic Ocean in the 21st century. *Journal of Geophysical Research: Oceans*, *123*(12), 9232–9244. https://doi.org/10.1029/2018JC014036

Smirnova, M. A., Kazarina, G. K., Matul, A. G., & Max, L. (2015). Diatom evidence for paleoclimate changes in the northwestern Pacific during the last 20000 years. *Oceanology*, *55*(3), 383–389. https://doi.org/10.1134/S0001437015030157

Stabell, B. (1986). A diatom maximum horizon in upper Quaternary deposits. *Geologische Rundschau*, *75*(1), 175–184. https://doi.org/10.1007/BF01770186

Stabeno, P. J., & Reed, R. K. (1994). Circulation in the Bering Sea Basin observed by satellite-tracked drifters: 1986-1993. *Journal of Physical Oceanography*, *24*(4), 848–854. https://doi.org/10.1175/1520-0485(1994)024<0848:CITBSB>2.0.CO;2

Stabeno, P. J., Schumacher, J. D., & Ohtani, K. (1999). The physical oceanography of the Bering Sea. In T. R. Loughlin, & K. Ohtani, (Eds.), *Dynamics of the Bering Sea: A summary of physical, chemical, and biological characteristics, and a synopsis of research on the Bering Sea* (pp. 1–28). University of Alaska Sea Grant, Fairbanks North Pacific Marine Science Organization. Retrieved from https://www.pmel.noaa.gov/pubs/outstand/stab1878/stab1878.shtml

Stoof-Leichsenring, K. R., Epp, L. S., Trauth, M. H., & Tiedemann, R. (2012). Hidden diversity in diatoms of Kenyan Lake Naivasha: A genetic approach detects temporal variation. *Molecular Ecology*, *21*(8), 1918–1930. https://doi.org/10.1111/j.1365-294X.2011.05412.x

Syvertsen, E. E. (1991). Ice algae in the Barents Sea: Types of assemblages, origin, fate and role in the ice-edge phytoplankton bloom. *Polar Research*, *10*(1), 277–288. https://doi.org/10.1111/j.1751-8369.1991.tb00653.x

Tremblay, J.-É., & Gagnon, J. (2009). The effects of irradiance and nutrient supply on the productivity of Arctic waters: A perspective on climate change. In J. C. J. Nihoul, & A. G. Kostianoy, (Eds.), *Influence of climate change on the changing arctic and sub-arctic conditions* (pp. 73–93). Springer Netherlands. https://doi.org/10.1007/978-1-4020-9460-6_7

Vincent, F., & Bowler, C. (2020). Diatoms are selective segregators in global ocean planktonic communities. *mSystems*, *5*(1). https://doi.org/10.1128/mSystems.00444-19

von Quillfeldt, C. H. (1997). Distribution of diatoms in the Northeast Water Polynya, Greenland. *Journal of Marine Systems*, *10*(1), 211–240. https://doi.org/10.1016/S0924-7963(96)00056-5

von Quillfeldt, C. H. (2000). Common diatom species in Arctic spring blooms: Their distribution and abundance. *Botanica Marina*, *43*(6), 499–516. https://doi.org/10.1515/BOT.2000.050

Walsh, J. E., Fetterer, F., Scott stewart, J., & Chapman, W. L. (2017). A database for depicting Arctic sea ice variations back to 1850. *Geographical Review*, *107*(1), 89–107. https://doi.org/10.1111/j.1931-0846.2016.12195.x

Zimmermann, H. H., Raschke, E., Epp, L. S., Stoof-Leichsenring, K. R., Schwamborn, G., Schirrmeister, L., et al. (2017). Sedimentary ancient DNA and pollen reveal the composition of plant organic matter in Late Quaternary permafrost sediments of the Buor Khaya Peninsula (north-eastern Siberia). *Biogeosciences*, *14*(3), 575–596. https://doi.org/10.5194/bg-14-575-2017

Zimmermann, H. H., Stoof-Leichsenring, K. R., Kruse, S., Müller, J., Stein, R., Tiedemann, R., & Herzschuh, U. (2019). Changes in the composition of marine and sea-ice diatoms derived from sedimentary ancient DNA of the eastern Fram Strait over the past 30,000 years. *Ocean Science Discussions*, 1–25. https://doi.org/10.5194/os-2019-113

Zimmermann, H. H., Stoof-Leichsenring, K. R., Kruse, S., Müller, J., Stein, R., Tiedemann, R., & Herzschuh, U. (2020). *Diatom sedimentary ancient DNA metabarcoding from western Fram Strait and Kronotsky Peninsula*. Dryad, Dryad Dataset. https://doi.org/10.5061/dryad.bnzs7h481

Zimmermann, H. H., Stoof-Leichsenring, K. R., Kruse, S., Nuernberg, D., Tiedemann, R., & Herzschuh, U. (2020). *Diatom sedimentary ancient DNA metabarcoding from Kronotsky Peninsula*. Dryad, Dryad Dataset. https://doi.org/10.5061/dryad.qnk98sfdh

Zimmermann, J., Abarca, N., Enk, N., Skibbe, O., Kusber, W.-H., & Jahn, R. (2014). Taxonomic reference libraries for environmental barcoding: A best practice example from diatom research. *PLOS One*, *9*(9), e108793. https://doi.org/10.1371/journal.pone.0108793